Peridynamic simulation of dynamic fracture in functionally graded materials subjected to impact load

Adem Candaş[a]*, Erkan Oterkus[b], C. Erdem İmrak[a]

[a] Faculty of Mechanical Engineering, Istanbul Technical University, Beyoğlu, Istanbul, 34437, Turkey

[b] Department of Naval Architecture, Ocean and Marine Engineering, University of Strathclyde, Glasgow G4 0LZ, United Kingdom

*Corresponding author: candas@itu.edu.tr

Abstract

Dynamic crack propagation assessment in functionally graded materials (FGMs) with micro-cracks is accomplished using bond-based Peridynamics (PD). The dynamic fracture behaviour of various FGMs' material models is studied in Kalthoff-Winkler experiment. Dynamic crack growth predictions and associated material damage of the specimen under dynamic loading conditions are considered. The effect of micro-cracks near macro-crack tips on the toughening mechanism is evaluated in terms of crack propagation velocities. Stochastically pre-located micro-cracks are modelled to obtain the toughening effect in the material. Additionally, the velocities and time required for fracture are compared in different FGM cases. It is frankly found that if a crack propagates in the harder region of the specimen, velocities decrease and toughness increase in contrast to the softer region. Furthermore, micro-cracks around a macro-crack decelerate the crack propagation and enhance toughening mechanism in FGM body depending on gradation of material properties.

Keywords: Crack propagation; functionally graded materials; material toughness; Kalthoff Winkler; Peridynamics.

This is a peer-reviewed, accepted author manuscript of the following article: Candas, A., Oterkus, E., & Imrak, C. E. (Accepted/In press). Peridynamic simulation of dynamic fracture in functionally graded materials subjected to impact load. Engineering with Computers.

1 Introduction

Recent progress and trends in material science and manufacturing technologies have led to a proliferation of studies and broad application areas on functionally graded materials (FGMs). FGMs are considered as composites whose material properties are changing with specific functions in any determined direction. They are nonhomogeneous materials and consist of two different types of materials such as ceramics, steel, and aluminium. The composition of two materials improves material properties in terms of strength, light weight, and resistance to impact loading. Moreover, the continuous differentiation of material properties prevents discontinuity problems arising in interface regions of composite materials. There are various studies on static analysis of FGMs such as using the mixed type Finite Element Method (FEM) with a functional [1–3], various material couples for functionally graded beams using high-order variational FEM [4] and neural networks by FEM [5]. Various analytical and numerical approaches to the static analysis of FGM are proposed in [6, 7]. Understanding the effect of defects that pre-existed or formed during operation in FGMs is essentially important during any material selection and design phases. In last few decades, there has been a surge of interest in crack initiation and propagation and related dynamic fracture problems on these materials (see, e.g. [8–12]). More recently, there has been a growing number of publications focusing on dynamic fracture problems in FGMs. Dynamic analysis of failure in an FGM subjected to impact load has been presented in, e.g. [12–14], and crack propagation analysis has been studied in [15–20].

The asymmetrical material properties of FGMs may lead to complex crack propagation in a structure [21]. Many authors have carried out a series of experiments to understand the crack propagation mechanisms. Jin et al. [22] examined the fracture response of FGMs and found that the non-uniform material properties could only lead to a local distortion on crack propagation. Abanto-Bueno and Lambros [23] performed fracture experiments to evaluate quasi-static mixed mode crack initiation and propagation in FGMs. Jain and Shukla [24] examined the dynamic fracture behaviour of FGMs subjected to mixed mode load. Kirugulige and Tippur [25] investigated crack initiation, path, and

speed in a glass-filled epoxy sheet under dynamic loading conditions. Rousseau and Tippur [26] investigated the crack tip behaviour in a compositionally graded glass-filled epoxy under low-velocity impact loading by experimentation. Toktas and Dag [27] presented an analysis of an inclined surface crack in an FGM under contact loading. Shukla et al. [28] presented a comprehensive review of dynamic fracture studies in FGMs.

Nearly all studies of simulating dynamic fracture behaviour of materials have been carried out using Finite Element Method (FEM) with certain modifications such as cohesive-zone [29], element-erosion [30], and extended-FEM (XFEM) [31]. The element-erosion and cohesive-zone techniques might not obtain exact results since crack propagation can only advance through element boundaries [32]. Although some studies [33–36] have proposed that XFEM is an effective method for numerical modelling of crack propagation, it has a certain limitation in adjusting the input fracture energy to obtain accurate results [32]. Rabczuk et al. [37] and Kosteski et al. [38] examined the crack propagation problem with discrete element models. Moreover, a 2D discrete model was presented by Braun and Fernández-Sáez [39]. On the other hand, Kim and Paulino [40] presented a remeshing algorithm with FEM to model crack propagation in FGMs under mixed-mode loading. Finally, Kirugulige and Tippur [41] adopted the cohesive elements in FEM, based on a bilinear traction-separation law, to explore material gradation's effect on crack propagation. However, all stated methods that used classical continuum mechanics suffer from serious shortcomings such as lattice or mesh dependency. Moreover, using partial differential equations requires specific special treatments in describing discontinuities such as cracks.

Silling [42] presented Peridynamics (PD) approach as a non-local form of the continuum mechanics. Silling and Askari [43] established PD theory that naturally overcomes the discontinuity issues in classical continuum mechanics. The crack modelling, nucleation, and propagation were naturally involved in PD owing to its integral form in contrast to the classical approach's local differential form. In PD theory, a continuum body is transferred into discretised material points having volumes

in space. Material points have been considered in interaction with other points located within a certain radius, termed the horizon. The behaviour of a material point is determined by other points in its horizon. PD formulation based on integro-differential equations complies with models comprising discontinuities such as cracks [42]. Silling and Lehoucq [44] tested the theory's robustness and efficiency, comparing the force densities of PD and classical elasticity theory. A considerable amount of studies using PD have been published, such as combining PD and FEM [45, 46], the effect of corrosion pits on crack propagation [47], Hookean type membrane deformation under different loading conditions [48], fracture in polycrystalline materials [49], modelling of explosive loading on composite laminates [50], a geometrically exact formulation of PD [51], and plate deformations [52, 53]. Besides, PD has been implemented in various applications such as flat shells under in-plane loading [54], extended non-ordinary state-based PD [55], effect of porosity on fatigue nucleation [56], crack growth modelling during fatigue [57], and higher order FGMs [58]. Madenci and Oterkus' book [59] presents a comprehensive explanation of the PD theory giving various examples and applications. Javili et al. [60] presented a comprehensive review evaluating different applications of PD.

Some authors [61–63] have investigated micro/macro- crack interaction using analytical methods. A bimaterial consisting of homogeneous materials and an FGM media containing multiple cracks were examined and compared in [64]. Singh et al. [65] examined multiple regularly located cracks, holes and inclusions and their interactions with a macro-crack in an FGM body. On the other hand, recent studies using PD have ensured the analysis of more complex micro-crack patterns and provided reliable crack propagations. Vazic et al. [66] examined the crack advancing and branching affected by micro-cracks regularly located around the main crack tip. Basoglu et al. [67] compared various micro-crack patterns around the main crack tip and examined the micro-crack toughening mechanism. Numerous studies, e.g. [68–72], have shown the applicability of PD theory on crack initiation and propagation in dynamic loading and thermo-mechanics problems. Both Ghajari et al. [73] and Ozdemir et al. [74] applied PD theory to analyse functionally graded materials. They investigated

dynamic crack propagation and wave propagation in a 2D rectangular body. Moreover, He et al. [75] modelled thermal shock loading using PD in FGMs. Candaş et al. [76] examined the effect of the stochastically distributed micro-cracks around the macro-crack tip on the material toughening mechanism and used PD theory to simulate the crack propagation in Kalthoff Winkler experiment [77, 78], and proposed a two-dimensional micro-crack definition. Kalthoff-Winkler experiment has been broadly studied in the literature and therefore is an excellent candidate to examine the crack propagation and toughening mechanism hypothesis in FGMs. So far, a number of studies have examined the Kalthoff-Winkler problem using PD such as a validation study of PD [79], dual horizon PD formulation [80, 81], state-based PD for thermoplasticity [82], implementing non-uniform discretization [83], investigation of model dimensions and parameters [84], meshfree quadrature rule for PD [85], and reformulated thermo-visco-plastic model [86]. Despite well-studied dynamic crack propagation in both homogeneous and FGMs, several questions remain to be answered about the effect of micro-cracks on crack propagation in FGMs. The examination of crack propagation and its interaction with micro-cracks in a functionally graded material subjected to impact load stands out as a gap in the literature that needs further investigation. This study seeks to obtain data which will help to address the effect of FGM properties and pre-located micro-cracks on toughening mechanism. Hence, the authors applied a gradation effect to material properties of the body used in the Kalthoff-Winkler problem and concentrated on the crack propagation in the dynamic fracture of FGMs using bond-based PD. Determining the effect of pre-located micro-cracks on the toughening mechanism in a three-dimensional FGM body is considered as a novel approach. After briefly explaining the bond-based PD theory, two-dimensional micro-crack definition and functionally graded material adaptation have been defined. In this paper, the proposed method has been applied to Kalthoff-Winkler impact problem and numerical results have been obtained and discussed.

2 Methodology

In this section, firstly fundamentals of PD theory are introduced. The equation of motion in PD, the discretized form, and the failure definition are given. Then, micro-crack definition used in the study is explained. Finally, the adaptation of FGM modelling parameters to PD is presented.

2.1 Peridynamic formulation

During the last decade, modelling of dynamic fracture problems using PD has been at the centre of much attention. To overcome discontinuity issues in classical continuum mechanics, Silling [42] presented PD theory that is applicable in discontinuous regions, e.g. zones in which a crack is forming and propagating in a material. The equations based on partial derivatives are invalid in discontinuity regions. On the contrary, the equation of motion in PD is valid in both continuity and discontinuity regions in material because it is based on integral equations. Silling [42] firstly presented bond-based PD theory in the form of which force density vectors between two material points are parallel and equal in magnitude. Silling et al. [87] extended this formulation to the state-based PD theory that uses unequal force density vectors. The integral based equation of motion in PD theory for any material point $\mathbf{x}$ is defined as [43]

$$\rho\ddot{\mathbf{u}}(\mathbf{x},t)=\int_{\mathcal{H}_{\mathbf{x}}}\mathbf{f}(\mathbf{u}(\mathbf{x}',t)-\mathbf{u}(\mathbf{x},t),\mathbf{x}'-\mathbf{x})\mathrm{d}V_{\mathbf{x}'}+\mathbf{b}(\mathbf{x},t)\,, \tag{1}$$

where $\mathbf{x}'$ is the family member inside the horizon $\mathcal{H}_{\mathbf{x}}$. The radius of the spherical horizon region is δ. The force vector, $\mathbf{f}$ is the mutual force between two material points $\mathbf{x}$ and $\mathbf{x}'$. $\mathbf{u}$ is the displacement vector, $\mathbf{b}$ is the body load, ρ is the mass density, and $\mathrm{d}V_{\mathbf{x}'}$ is the infinitesimally small volume of point $\mathbf{x}'$. In Fig. 1, position vectors, $\boldsymbol{\xi}=\mathbf{x}'-\mathbf{x}$ represents the relative positions in reference state and $\boldsymbol{\eta}+\boldsymbol{\xi}=\mathbf{y}'-\mathbf{y}$ denotes the relative positions of material points after deformation, where $\boldsymbol{\eta}=\mathbf{u}(\mathbf{x}',t)-\mathbf{u}(\mathbf{x},t)$ is the relative displacement vector [43, 59]. Considering the relative displacement between material points, the stretch of a bond is expressed as follows,

$$s=\frac{(\mathbf{y}'-\mathbf{y})-(\mathbf{x}'-\mathbf{x})}{\mathbf{x}'-\mathbf{x}}=\frac{|\boldsymbol{\xi}+\boldsymbol{\eta}|-|\boldsymbol{\xi}|}{|\boldsymbol{\xi}|}. \tag{2}$$

This equation defines the bonds between two material points as an elastic spring in a micro-elastic material. Thus, a scalar micro-potential function in a bond according to the bond-based Peridynamics is

$$w(\boldsymbol{\eta},\boldsymbol{\xi}) = \frac{1}{2} c s^2 |\boldsymbol{\xi}|, \tag{3}$$

where the bond constant, $c = 12E/\pi\delta^4$ is expressed for three-dimensional structures in terms of elastic modulus, E and the radius of horizon, δ [59]. The pairwise force function **f**, is the derivative of micro-potential function with regard to the relative displacement vector:

$$\mathbf{f}(\boldsymbol{\eta},\boldsymbol{\xi}) = \frac{\partial w}{\partial \boldsymbol{\eta}}(\boldsymbol{\eta},\boldsymbol{\xi}) = \frac{\boldsymbol{\xi}+\boldsymbol{\eta}}{|\boldsymbol{\xi}+\boldsymbol{\eta}|} f(|\boldsymbol{\xi}+\boldsymbol{\eta}|,\boldsymbol{\xi}) \quad \forall\, \boldsymbol{\eta},\boldsymbol{\xi}, \tag{4}$$

where f is a scalar-valued function in terms of the bond constant and bond stretch. The bond between two material points is valid only if the initial reference distance between these points is within the horizon that restricts the interaction of material points with others. Therefore, the scalar-valued force function between material points is defined as:

$$f(|\boldsymbol{\xi}+\boldsymbol{\eta}|,\boldsymbol{\xi}) = \begin{cases} cs\mu(t,\boldsymbol{\xi}) & \text{if } |\boldsymbol{\xi}| < \delta \text{ for all } \boldsymbol{\eta}, \\ 0 & \text{otherwise} \end{cases} \tag{5}$$

where $\mu(t,\boldsymbol{\xi})$ is a history-dependent scalar-valued step function to ensure that the bond-stretch s, does not exceed a pre-defined critical-stretch value s_c. This condition also provides a failure criterion in PD by considering the bond is not recoverable after failure. The function $\mu(t,\boldsymbol{\xi})$ is valued as 1 if the bond-stretch $s(t',\boldsymbol{\xi})$ is smaller than the critical-stretch s_c over time, otherwise it is evaluated as 0 that means breaking a bond between two material points. Overall, in PD theory, the force between two material points can only be defined if these points are within the horizon and vanish after bond-stretch exceeding the critical-stretch value. These definitions provide PD theory deals with discontinuities in a continuous body. Both pre-defined cracks and crack propagation can be modelled by eliminating bonds through the crack surface. The pre-defined critical-stretch value is defined in [59] as follows,

$$s_c = \sqrt{\frac{G_c}{\left(3\mu + \left(\frac{3}{4}\right)^4 \left(\kappa - \frac{5\mu}{3}\right)\right)\delta}}, \tag{6}$$

where G_c is the critical energy release rate, κ is bulk modulus, and μ is the shear modulus. Considering the broken bonds for a material point, the local damage parameter can be written as

$$\varphi(\mathbf{x}, t) = 1 - \frac{\int_{\mathcal{H}_\mathbf{x}} \mu(\mathbf{x}, t, \boldsymbol{\xi})\, \mathrm{d}V_\xi}{\int_{\mathcal{H}_\mathbf{x}} \mathrm{d}V_\xi}. \tag{7}$$

This equation is the weighted ratio of the number of damaged bonds to the entire internal interactions for a material point.

The integral based equation of motion in PD is not usually solved by analytical tools. Therefore, the continuum body is re-defined as discretized volumes that have certain volumes to obtain a numerical solution. The governing equation for a material point *k* by taking into account all points in its horizon is given in a discretized form:

$$\rho_k \ddot{\mathbf{u}}_k^n = \sum_j \mathbf{f}\left(\mathbf{u}_j^n - \mathbf{u}_k^n, \mathbf{x}_j - \mathbf{x}_k\right) V_j + \mathbf{b}_k^n . \tag{8}$$

The displacement vector is represented by $\mathbf{u}_k^n$ for a material point *k* at the time step, n^{th}. The constant grid spacing is denoted by Δx and the volume of material point *j*, is defined as $V_j = (\Delta x)^3$ in a three-dimensional body [43].

2.2 Micro-crack definition

Both macro- and micro- level pre-existed defects have always been a problematic issue for materials under impact load. These cracks that are located in material with various positions, angles, and lengths may cause high stress concentrations around the crack tips. Micro-cracks are relatively smaller cracks with regard to existing macro-cracks in a structure. Vazic et al. [66] defined micro-cracks as

$l_{micro-crack} = l_{macro-crack}/50$ for a plate. Basoglu et al. [67] considered a similar approach and defined micro-cracks as $l_{micro-crack} = l_{macro-crack}/50$ and $l_{micro-crack} = l_{macro-crack}/25$ for a plate with the size of 0.05×0.05 m^2 that contain a macro-crack with the length of 0.025 m. In our previous study [76], we defined the length of micro-cracks as $l_{micro-crack} = l_{macro-crack}/16$ in a body with the size of 0.1×0.2 m^2. In three-dimensional body, micro-cracks are considered as a plane passing through all material with a thickness of 0.009 m. We applied the same proportion for the purpose of results comparison with reference [76]. PD has a straightforward approach to define a realistic model for creating micro-cracks. Madenci and Oterkus [59] showed that the damage value for material points can be calculated quantitively in terms of the local damage. They examined the damage of a material point with respect to the location of crack surface. The pre-defined crack line in a two-dimensional discretised body is given as a red line in Fig. 2. When bonds of material points intersect with the crack line, the bond-breakage occurs. The position of crack line may be adjusted in any location between material points to obtain particular crack surfaces in many numbers. Thus, bonds between the material point and its family members are diminished with regard to the length of crack. The colour scale shows percentages of damaged material points' bonds. The amount of damage is affected by the proximity to crack line. The points closest to the crack has been damaged more than distant ones. While the material point A has lost 40% of its bonds, the material point B has lost 22% of its bonds. We have applied the flowchart in Fig.3 in [76] to create a body that suffer from multiple micro-cracks. This algorithm can be applied for any type of Peridynamic codes in any application. It starts with defining coordinates and length of a single micro-crack. The next step is finding material points that their horizon intersects with the crack. Then, if the bond between the determined material point and its family member intersects with the crack, the bond is considered broken. The number of broken bonds determines the damages.

2.3 Peridynamic formulation for FGMs

The combination of two materials in composite materials to improve strength and stiffness leads to an uncertainty in material properties at the transition zones. Functionally graded materials overcome this issue by a smooth differentiation in material properties in any direction. Moreover, gradient structure provides a continuous variation in material properties such as strength and toughness. FGMs can be designed according to direction of applied loads.

The adaptation of FGMs in bond based Peridynamic theory needs special treatment and assumptions to determine material properties, such as elastic modulus and critical energy release rate. In Eq. (5), the scalar-valued force function is expressed in terms of bond stretch and also bond constant that is a function of elastic modulus and horizon radius. The horizon radius is a PD model parameter that is not changing with material properties. On the other hand, considering the elastic modulus is changing differentially along a direction in an FGM body, the bond constant shall be determined for each particular bond between a material point and its neighbour in the horizon. To determine a bond constant for each material point in a discretized body, the following averaging formula is adopted as

$$c' = \frac{12}{\pi\delta^4}\left(\frac{E_j + E_k}{2}\right), \tag{9}$$

where, c' presents a value for a particular bond in a certain horizon depending on E_j and E_k that are elastic modulus of material points $\mathbf{x}_j$ and $\mathbf{x}_k$ at each end of the bond. The same approach should be applied to the critical bond stretch, s_c for modelling of FGMs in PD. In the formula of critical stretch (Eq. (6)), the horizon radius, δ is not dependent on material properties. However, bulk modulus, κ and shear modulus, μ differentiate depending on elastic modulus, E because of constraints in bond based Peridynamic theory. In addition, the critical energy release rate, G_c is a material property that gradually changes in FGMs. The variation of the critical stretch, s_c' for each bond between material points is expressed as,

$$s_c' = \sqrt{\frac{G_c'}{\left(3\mu' + \left(\frac{3}{4}\right)^4 \left(\kappa' - \frac{5\mu'}{3}\right)\right)\delta}}, \tag{10}$$

where, the mean value of critical energy release rate is $G_c' = \left(G_{c,j} + G_{c,k}\right)/2$, bulk modulus is $\kappa' = \left(\kappa_j + \kappa_k\right)/2$, and shear modulus $\mu' = \left(\mu_j + \mu_k\right)/2$ with the constraint conditions $\kappa = 5\mu/3$ or $\nu = 1/4$ emerging from bond-based Peridynamics [59]. The gradual differentiation of material properties and its effect on critical stretch and bond constant is represented schematically in Fig. 3. The practical advantage of using this straightforward approach is that it provides a control of material properties for each discretised material point in PD.

3 Numerical examples

Numerical examples were considered on Kalthoff-Winkler problem that adapted FGMs. In Section 1, the original experiment performed by Kalthoff and Winkler [77] was given as a reference model. After that, material properties proposed by Zhang et al. [88] were modified to be used in Kalthoff-Winkler problem. The "softer" and "harder" materials that were defined in [88] were adapted as homogeneous cases for the purpose of benchmarking. In Section 3.2, a linear gradation effect on material properties was applied in parallel to the direction of impact load to compare homogeneous and FGM characteristics. In Section 3.3, FGM properties proposed by Kirugulige and Tippur [25] and used in [68] were implemented in Kalthoff-Winkler problem. Finally, in Section 3.4, the effect of micro-cracks on the crack propagation in FGM models was also presented. The software package OVITO [89] is used for visualization.

Kalthoff and Winkler carried out a series of impact tests on a high-strength maraging steel plate (X2NiCoMo 18 9 5) containing two parallel notches and performed outstanding experiments on the impact loading and mode transitions on a crack propagation problem [77, 78, 90, 91]. A steel impactor impacts with a constant velocity in parallel direction to notches as shown in Fig. 4. The homogenous

material properties of the plate are given in [59] and presented in Table 1. Kalthoff [78] explained the material behaviour of high-strength maraging steel under certain impact loading conditions as almost linear-elastic and it can be said that the stress distributions around the crack tip were modelled with linear-elastic equations. The Mode II crack propagation is almost parallel to notches because of shear bands controlling the fracture at high loading rates. Besides, a mode transition is observed at low rates of loading. Silling [79], therefore, stated that micro-elastic PD theory performs a suitable performance on simulating brittle fracture and crack propagation.

The cylindrical projectile impacts with a constant velocity to the target body and this results in a brittle fracture as stated in [77]. Hence, this paper only focused on the dynamic fracture analysis. As depicted in Fig. 4, dimensions of the experimental setup are $L = 0.200$ m, $W = 0.100$ m, and $t = 0.009$ m. The distance between symmetrically located notches is $d = 0.050$ m with a length of $a = 0.050$ m. The thickness of the notches is $n = 0.0015$ m. During the simulations, plates are traction-free and at rest. The projectile is assumed as a rigid body with properties; $D = \phi 0.050$ m, $H = 0.050$ m and, m = 1.57 kg. The velocity is constant during simulations and directed into parallel to the notches as $v = -32$ m/s through the y-axis.

The steel plate body is discretized with $201 \times 101 \times 9$ material points along x, y, and z-axes, respectively. The grid size (spacing between material points) is specified as $\Delta = 0.001\, m$ in each direction and the total number of material points is 180,873. The horizon's radius is $\delta = 3.015 \times \Delta$ as given in [59]. The time-step is $\Delta t = 8.7 \times 10^{-8}$s and the reference critical- stretch is $s_c = 0.01$ defined as in [59].

3.1 Benchmark tests

A series of numerical tests for examining dynamic crack propagation in both homogeneous and FGMs were performed by Zhang et al. [88]. They proposed two models considering linearly graded Young's modulus E, and critical energy release rate G_c to obtain material properties differentiation in direction

of the impact load. In the benchmark problem, the "softer" and "harder" material properties that defined in [88] were adapted to test the applicability of proposed methodology. The softer and harder terms refer to low and high Young's modulus and critical energy release parameters, respectively, as defined in [88]. In Table 1, material properties of the reference state (M1), and proposed cases, M2 and M3 are given. Note that M2 and M3 models are homogeneous models. In these models, Young's modulus and critical energy release parameters are altered by $\pm 33\%$ from the reference values. The Poisson's ratio is taken as constant, $\nu = 1/4$. Due to the relation between Young's Modulus and critical energy release rate in Eq. (6), the critical stretch value remains constant. Likewise, the mass density is $\rho = 8000\ \mathrm{kg/m^3}$. In the reference model M1 produced from the original experiments in [77], notches dominate the crack initiation location and propagation direction. The propagation initiates at 30.5 μs (350th timestep). The complete fracture occurs by reaching cracks to both ends at 91.4 μs (1050th timestep). All models in this study were run to 117.5 μs (1350th timestep) to obtain a fully occurred separation in the body. In the benchmark models M2 and M3, cracks start to initiate at 30.5 μs as same as the reference model M1. However, the cracks cannot reach the edges at 91.4 μs in M2 case, because of the decrease in crack propagation velocity. The complete fracture occurs at 104.4 μs with a 13.0 μs time delay. On the contrary, cracks in M3 case reach the edges at 87.0 μs. Thus, the crack paths for M1, M2, and M3 cases are given at 87.0 and 104.4 μs in Fig. 5. Crack lengths are calculated by taking the difference between the first and last coordinates of cracks. Considering the crack initiation and complete fracture, the average velocities are 1253, 958, and 1389 m/s for M1, M2, and M3 cases, respectively, in between time interval 30.5 - 87.0 μs. Herein, the crack propagation velocity of M2 reduced about 24% as compared with the reference model M1 while the average velocity in M3 increased about 11%. Velocity profiles for models are shown in Fig. 6. These results are presented by adapting the homogeneous material properties for the two material models given in [88]. The results of the benchmark study based on these homogeneous material models show the applicability of our PD theory with different Young's modulus and critical energy release rate.

3.2 Comparison of homogenous material and FGMs

The challenging work for the adaptation of FGMs in PD theory is the calculation of each varying properties of bonds as given in Eq. (9). M2 and M3 were homogenous models. The purpose of this section is that examining the effect of linearly changed Young's modulus and critical energy release rate. Thus, with the same values in the benchmark study, two different FGM models are defined: M4 and M5. The maximum and minimum values of material properties of M4 and M5 are given in Table 1. In the first model, Young's modulus varies linearly through *y*- direction from $E_{y=0} = 127$ to $E_{y=0.1} = 255$ GPa. Also, the critical energy release rate varies linearly from $G_{c,y=0} = 46.1$ to $G_{c,y=0.1} = 92.1\ \mathrm{kJ/m^2}$. In the reference model M1, $E = 191$ GPa and $G_c = 69.1\ \mathrm{kJ/m^2}$ are the constant properties. The linear relationship between E and G_c results in constant critical stretch values for each bond. The model M5 is a reverse-valued setup with regard to M4 model. The summary of all material properties data is given in Table 1. The results of the M4 and M5 models are used to compare the crack propagation velocity of the reference case. In Fig. 7, the simulation of the reference model and FGM models are given to compare the velocities obtained from simulations. While cracks in the reference model M1 and FGM model M4 start to initiate propagation 30.5 μs (350th timestep), the other FGM model M5 has a delay of about 4.3 μs. Considering the time for cracks reaching edges, the delay in the crack initiation time shows its effect on M5 model. The complete fracture occurs in M1 (Fig. 7 (a)) and M4 (Fig. 7 (c)) models at 91.4 μs, whereas 95.7 μs in M5 (Fig. 7 (f)) model. The average velocities are 1253, 1354, and 1064 m/s for M1, M4, and M5 models, respectively in between time interval 30.5 - 87.0 μs. It can be seen that the average velocities are changing depending on the gradation direction of material properties. The propagation of crack changes; moreover, the crack path angles have been affected as shown in Fig 7 (f). Although patterns in all simulations are nearly straight and very similar to patterns in [59, 81, 84], the change of direction in propagation can be observed. Zhang et al. [88] emphasized that propagation showed a tendency to advance into the weaker areas and explained this phenomenon by the fact that the stiffness between impacted surface (*y=0.1*) and the crack tip is greater than the other cases. As a result of this difference, the average velocity in M4 model increased about 8% as compared with the reference model M1. Moreover, the

directions of crack tips direction become different for all three cases as shown in Fig. 7 (f). The velocity profiles of M4 and M5 models are given with previous models in Fig 6. These alterations in both direction and velocity changes are consistent with that of Zhang et al. [88] performed by using Cohesive Zone Model approach.

3.3 More comprehensive PD FGM model

Models considered so far provide some results concerning the FGMs modelling. The lack of all material properties that affect the dynamic crack propagation requires the need for more simulations. What remains unclear, however, is whether the crack propagation is affected by other parameters such as fracture toughness, critical stretch, and mass density. The extent to which material properties moderate crack propagation is still unclear. In the previous section, the effect of Young's modulus and critical energy release rate are examined. Here, the effect of fracture toughness, critical stretch, and mass density are also taken into account in this section.

Kirugulige and Tippur [41] carried out a series of dynamic crack experiments on a brittle FGM plate containing a crack. After the observation, they developed a finite element model with cohesive elements to explain the material gradation effect. The given linear variation of parameters; Young's modulus, fracture toughness, and mass density were also used in [68] for examining dynamic crack propagation using PD and in [74] for studying crack branching in FGMs. Following linear equations for material properties gradation in Kalthoff-Winkler experiment were adapted from [41, 68, 74] to set up an analogy that develops a similar FGMs behaviour.

$$K_C(y) = 140.2 - \frac{140.2 - 89.6}{0.1} y \qquad 0 \le y \le 0.1 \text{ m}, \tag{11}$$

$$E(y) = 271 - \frac{271 - 111}{0.1} y \qquad 0 \le y \le 0.1 \text{ m}, \tag{12}$$

$$\rho(y) = 9600 - \frac{9600 - 6400}{0.1} y \qquad 0 \le y \le 0.1 \text{ m}, \tag{13}$$

$$G_C(y) = \frac{K_{IC}^2(y)}{E(y)}. \tag{14}$$

In the above equations, y is varied from 0 to 0.1 m. The units for fracture toughness $K_{IC}(y)$, Young's modulus $E(y)$, and mass density $\rho(y)$ are MPa $\cdot \sqrt{\text{m}}$, GPa and kg/m^3, respectively. Because of the transitions between Mode I and Mode II fracture mechanisms in Kalthoff-Winkler experiment [78], a difficulty arises to determine critical energy release rates for Mode I (G_{IC}) and Mode II (G_{IIC}). Kirugulige and Tippur [41] stated that the equality of $G_{IC} = G_{IIC}$ was used due to the lack of application of pure Mode II experiments under dynamic loading conditions. Therefore, with the plane stress assumption suggested in [41], the critical energy release rate is determined by Eq. (14). This approach was also used in [68, 74]. The reference value $E = 191$ GPa is changed by $\pm 42\%$ to obtain limit values of E as in accordance with [41]. The reference values of K_{IC} and ρ are changed by $\pm 22\%$ and $\pm 20\%$, respectively. The variation of Young's modulus, critical energy release rate, and mass density of M6 and M7 models examined in this section are shown in Fig. 8. Maximum and minimum values of all material properties are summarized in Table 1. Models M6 and M7 were compared to the reference model M1. While cracks start to propagate at 30.5 μs in M1 and M6 models, the initiation occurs at 34.8 μs in M7 model. In Fig. 9, crack positions of all models are given. It can be seen that cracks in M6 reach the edge within the same time (91.4 μs) according to the reference model M1. The model M7 is shown in Fig. 9 (e,f). When the tip of cracks at 91.4 μs is inspected in M7 model, decreasing in the crack velocity can be observed compared to M1 and M6 models. The complete fracture can only occur at about 100.1 μs. In Fig. 10, velocity profiles of models are presented. The average velocities in M1, M6, and M7 models are 1253 m/s, 1340 m/s, and 956 m/s, respectively. The offset on M7 compared to M1 model can be clearly seen, which results in about 24% decrease in average velocity. In M7 model, material properties linearly change from lower at the $y = 0.1$ m to higher values at $y = 0$. The propagation velocity appeared to be affected by stiffer material properties in the crack path. The velocities decelerate as they advance for all models. Cheng et al. [68, 69] also observed a similar velocity change in the stiffer side. These complete modelling

cases also provide a basis for the testing of the effect of micro-cracks on crack propagation in FGM body in the next section.

3.4 Randomly distributed micro-cracks in FGMs

In the section that follows, the effect of micro-cracks in the FGM body on the crack propagation velocity will be addressed. Micro-cracks around the crack tip may lead to micro-crack toughening effect in brittle materials due to crack shielding [63, 92, 93]. We previously examined this phenomenon in [76] to investigate relationship between randomly pre-located micro-cracks and the toughening mechanism in the Kalthoff–Winkler problem. Now, the model called A_2 in [76] that showed one of the most effective toughening effect is adapted in M6 and M7 models. In other words, models M8 and M9 have same material properties as M6 and M7, respectively. Moreover, they contain stochastically distributed micro-cracks. In addition to this modification, the A_2 model from [76], which had same homogeneous material properties as M1 model but with micro-cracks, is now examined as M1-w/mc (M1 with micro-cracks) model for comparison purposes. The crack locations, density and dimensions were presented in Fig. 10 in [76].

While cracks start to propagate at 30.5 μs in M1 and M1-w/mc models, the initiation occurs at 30.5 and 34.8 μs in M8 and M9 models, respectively. The crack initiation time in M8 and M9 are same as M6 and M7 models which means there is no significant effect on crack initiation arising from pre-located micro-cracks. The crack path location of simulations is given in Fig. 11 at times 91.4 and 100.1 μs. The complete fracture occurs in M8 at 95.7 μs with a delay of 4.3 μs with regard to M6 model. It should be mentioned that it is 91.4 μs in the reference model M1 (Fig. 11(a)). The required time for main-cracks to reach edges in M9 is 100.1 μs (Fig. (11(f)) which is the same as in M7. When considering the time for complete fracture in M1-w/mc is 104.4 μs, crack velocities in M8 and M9 seems slower than in M1-w/mc. However, required times for complete fracture may lead to a misinterpretation about the crack velocity and toughening effect due to changing of crack path's directions. Paths of crack propagations are given in Fig. 11 (f). Herein, average velocities should be

compared for all models. Since micro-cracks do not allow tracking the crack tip, velocities are evaluated once cracks pass over the micro-crack area. In Fig. 12, velocity profiles after 52.2 μs is given, in which the crack propagation is in the micro-crack-free area. Considering that cracks reach edges at 91.4 μs in M1 model, the velocity data should be compared up to this time. The average velocities between 52.2 and 91.4 μs are 1345, 1383, 1126, 1300, 1066, and 1219 m/s in models M1, M6, M7, M8, M9, and M1-w/mc, respectively. When FGM model M8 and homogenous model M1-w/mc are compared, the average velocity increases with application of FGM properties. On the other hand, FGM model M9 has lower average velocity value than M1-w/mc. This difference indicates that the direction of gradation of material points is an effective parameter on toughening mechanism in an FGM body with pre-located micro cracks around the crack tip. A possible cause of that crack propagation is in stiffer side of the body in M9 model with regard to M8 model. This also agrees with results stated by Zhang et al. [88]. Turning now to the comparison of FGM models with micro-cracks and without micro-cracks, there is a decrease in average velocity values in M8 and M9 models compared to M6 and M7 models. In that comparison, about 6% and 5% reductions in average velocities are obtained in M8 and M9 models. These results corroborate the findings of a great deal of the previous work in [76].

Overall, results in numerical examples chapter indicate that crack propagation shows various characteristics depending on material properties gradation in FGMs that both with and without micro-cracks. In summary, models M1, M2, and M3 are compared in Section 3.1. M1 is the original experimental setup. M2 and M3 are homogeneous material models. Crack propagation velocities are reduced with high Elastic modulus and critical energy release rate parameters, but increased with low ones. In Section 3.2, M4 and M5 FGM models with linearly changing material properties are presented and compared with M1 model. Here, crack propagations change depending on the gradation direction of material properties. If the crack propagation advances from stiffer part of the body to weaker, velocity of the propagation increases. In Section 3.3, M6 and M7 models considered variation of Elastic modulus, fracture toughness, critical energy release rate, and density. In Section 3.4, models

M8 and M9 have same material properties as M6 and M7, respectively, but they have pre-defined micro-cracks. M8 and M9 have lower crack propagation velocities than M6 and M7, respectively.

4 Conclusion

In this paper, the bond based Peridynamics (PD) model was presented to examine the crack propagation in a functionally graded material (FGM) body subjected to impact load and the effect of micro-cracks was investigated. Two FGM approaches have been adapted to obtain effects of material properties on the crack propagation. Material parameters such as Young's modulus, fracture toughness, and density gradation provides a more valid simulation approach to FGM modelling using PD. The most obvious finding to emerge from the analyses is that the softening of area without crack and hardening the area containing the crack path reduce the crack tip velocity and increase the toughness with an appreciable difference. One of the more significant verdicts to emerge from this study is that adding a pre-defined micro-crack cluster around the crack tip decelerate the crack propagation and cause toughening of an FGM body. However, there is a material gradation dependency on toughening mechanism when adding micro-cracks in FGMs. These results provide important insights into the role of micro-cracks and toughening effect in an FGM body. The results of this investigation complement those of earlier studies. This work contributes to existing knowledge of dynamic fracture mechanism in an FGM model by providing an investigation of toughening effect. Further research should be undertaken to explore how different material models affect the crack propagation under various impact states.

Acknowledgements

This research did not receive any specific grant from funding agencies in the public, commercial, or not-for-profit sectors.

Author Statement

AC: Visualization, Methodology, Software, Writing- Original draft preparation. **EO**: Software, Methodology, Reviewing and Editing, Supervision. **CEİ**: Methodology, Writing - Reviewing and Editing, Supervision.

References

1. Madenci E, Özütok A (2017) Variational Approximate and Mixed-Finite Element Solution for Static Analysis of Laminated Composite Plates. Solid State Phenom 267:35–39. https://doi.org/10.4028/www.scientific.net/SSP.267.35

2. Özütok A, Madenci E (2017) Static analysis of laminated composite beams based on higher-order shear deformation theory by using mixed-type finite element method. Int J Mech Sci 130:234–243. https://doi.org/10.1016/j.ijmecsci.2017.06.013

3. Madenci E, Özütok A (2020) Variational approximate for high order bending analysis of laminated composite plates. Struct Eng Mech 73:97–108. https://doi.org/10.12989/sem.2020.73.1.097

4. Madenci E (2021) Free vibration and static analyses of metal-ceramic FG beams via high-order variational MFEM. Steel Compos Struct 39:493–509. https://doi.org/10.12989/scs.2021.39.5.493

5. Madenci E, Gülcü Ş (2020) Optimization of flexure stiffness of FGM beams via artificial neural networks by mixed FEM. Struct Eng Mech 75:633–642. https://doi.org/10.12989/sem.2020.75.5.633

6. Madenci E (2019) A refined functional and mixed formulation to static analyses of fgm beams. Struct Eng Mech 69:427–437. https://doi.org/10.12989/sem.2019.69.4.427

7. Madenci E, Özkılıç YO (2021) Free vibration analysis of open-cell FG porous beams:

Analytical, numerical and ANN approaches. Steel Compos Struct 40:157–173. https://doi.org/10.12989/scs.2021.40.2.157

8. Delale F, Erdogan F (1983) The crack problem for a nonhomogeneous plane. J Appl Mech Trans ASME 50:609–614. https://doi.org/10.1115/1.3167098

9. Eischen JW (1987) Fracture of nonhomogeneous materials. Int J Fract 34:3–22. https://doi.org/10.1007/BF00042121

10. Jin ZH, Batra RC (1996) Some basic fracture mechanics concepts in functionally graded materials. J Mech Phys Solids 44:1221–1235. https://doi.org/10.1016/0022-5096(96)00041-5

11. Marur PR, Tippur H V. (2000) Numerical analysis of crack-tip fields in functionally graded materials with a crack normal to the elastic gradient. Int J Solids Struct 37:5353–5370. https://doi.org/10.1016/S0020-7683(99)00207-3

12. Itou S (2010) Dynamic stress intensity factors for two parallel interface cracks between a nonhomogeneous bonding layer and two dissimilar elastic half-planes subject to an impact load. Int J Solids Struct 47:2155–2163. https://doi.org/10.1016/j.ijsolstr.2010.04.020

13. Guo LC, Wu LZ, Ma L, Zeng T (2004) Fracture analysis of a functionally graded coating-substrate structure with a crack perpendicular to the interface - Part I: Static problem. Int J Fract 127:21–38. https://doi.org/10.1023/b:frac.0000035049.26772.2d

14. Ma L, Wu LZ, Guo LC (2005) On the moving Griffith crack in a nonhomogeneous orthotropic strip. Int J Fract 136:187–205. https://doi.org/10.1007/s10704-005-6023-z

15. Xia CH, Ma L (2007) Dynamic behavior of a finite crack in functionally graded materials subjected to plane incident time-harmonic stress wave. Compos Struct 77:10–17. https://doi.org/10.1016/j.compstruct.2005.05.012

16. Kidane A, Chalivendra VB, Shukla A, Chona R (2010) Mixed-mode dynamic crack propagation in graded materials under thermo-mechanical loading. Eng Fract Mech 77:2864–2880. https://doi.org/10.1016/j.engfracmech.2010.07.004

17. Cheng Z, Zhong Z (2007) Analysis of a moving crack in a functionally graded strip between two homogeneous layers. Int J Mech Sci 49:1038–1046. https://doi.org/10.1016/j.ijmecsci.2007.01.003

18. Cheng Z, Gao D, Zhong Z (2010) Crack propagating in functionally graded coating with arbitrarily distributed material properties bonded to homogeneous substrate. Acta Mech Solida Sin 23:437–446. https://doi.org/10.1016/S0894-9166(10)60046-8

19. Lee KH (2009) Analysis of a transiently propagating crack in functionally graded materials under mode I and II. Int J Eng Sci 47:852–865. https://doi.org/10.1016/j.ijengsci.2009.05.004

20. Matbuly MS (2009) Multiple crack propagation along the interface of a non-homogeneous composite subjected to anti-plane shear loading. Meccanica 44:547–554. https://doi.org/10.1007/s11012-009-9190-6

21. Hassan SF, Siddiqui O, Ahmed MF, Al Nawwah AI (2019) Development of gradient concentrated single-phase fine Mg-Zn particles and effect on structure and mechanical properties. J Eng Mater Technol Trans ASME 141:. https://doi.org/10.1115/1.4041865

22. Jin X, Wu L, Guo L, et al (2009) Experimental investigation of the mixed-mode crack propagation in ZrO2/NiCr functionally graded materials. Eng Fract Mech 76:1800–1810. https://doi.org/10.1016/j.engfracmech.2009.04.003

23. Abanto-Bueno J, Lambros J (2006) An experimental study of mixed mode crack initiation and growth in functionally graded materials. Exp Mech 46:179–196. https://doi.org/10.1007/s11340-006-6416-6

24. Jain N, Shukla A (2006) Mixed mode dynamic fracture in particulate reinforced functionally graded materials. Exp Mech 46:137–154. https://doi.org/10.1007/s11340-006-5867-0

25. Kirugulige MS, Tippur H V. (2006) Mixed-mode dynamic crack growth in functionally graded glass-filled epoxy. Exp Mech 46:269–281. https://doi.org/10.1007/s11340-006-5863-4

26. Rousseau CE, Tippur H V. (2001) Dynamic fracture of compositionally graded materials with cracks along the elastic gradient: Experiments and analysis. Mech Mater 33:403–421. https://doi.org/10.1016/S0167-6636(01)00065-5

27. Toktaş SE, Dag S (2020) Oblique surface cracking and crack closure in an orthotropic medium under contact loading. Theor Appl Fract Mech 109:102729. https://doi.org/10.1016/j.tafmec.2020.102729

28. Shukla A, Jain N, Chona R (2007) A Review of Dynamic Fracture Studies in Functionally Graded Materials. Strain 43:76–95. https://doi.org/10.1111/j.1475-1305.2007.00323.x

29. Lorentz E (2008) A mixed interface finite element for cohesive zone models. Comput Methods Appl Mech Eng 198:302–317. https://doi.org/10.1016/j.cma.2008.08.006

30. Unosson M, Olovsson L, Simonsson K (2006) Failure modelling in finite element analyses: Element erosion with crack-tip enhancement. Finite Elem Anal Des 42:283–297. https://doi.org/10.1016/j.finel.2005.07.001

31. Lancaster IM, Khalid HA, Kougioumtzoglou IA (2013) Extended FEM modelling of crack propagation using the semi-circular bending test. Constr Build Mater 48:270–277. https://doi.org/10.1016/j.conbuildmat.2013.06.046

32. Zhou X, Wang Y, Qian Q (2016) Numerical simulation of crack curving and branching in

brittle materials under dynamic loads using the extended non-ordinary state-based peridynamics. Eur J Mech A/Solids 60:277–299. https://doi.org/10.1016/j.euromechsol.2016.08.009

33. Moës N, Dolbow J, Belytschko T (1999) A finite element method for crack growth without remeshing. Int J Numer Methods Eng 46:131–150. https://doi.org/10.1002/(SICI)1097-0207(19990910)46:1<131::AID-NME726>3.0.CO;2-J

34. Belytschko T, Chen H, Xu J, Zi G (2003) Dynamic crack propagation based on loss of hyperbolicity and a new discontinuous enrichment. Int J Numer Methods Eng 58:1873–1905. https://doi.org/10.1002/nme.941

35. Zhuang Z, Cheng B Bin (2011) Development of X-FEM methodology and study on mixed-mode crack propagation. Acta Mech Sin Xuebao 27:406–415. https://doi.org/10.1007/s10409-011-0436-x

36. Wang H, Liu Z, Xu D, et al (2016) Extended finite element method analysis for shielding and amplification effect of a main crack interacted with a group of nearby parallel microcracks. Int J Damage Mech 25:4–25. https://doi.org/10.1177/1056789514565933

37. Rabczuk T, Zi G, Bordas S, Nguyen-Xuan H (2010) A simple and robust three-dimensional cracking-particle method without enrichment. Comput Methods Appl Mech Eng 199:2437–2455. https://doi.org/10.1016/j.cma.2010.03.031

38. Kosteski L, Barrios D'Ambra R, Iturrioz I (2012) Crack propagation in elastic solids using the truss-like discrete element method. Int J Fract 174:139–161. https://doi.org/10.1007/s10704-012-9684-4

39. Braun M, Fernández-Sáez J (2014) A new 2D discrete model applied to dynamic crack propagation in brittle materials. Int J Solids Struct 51:3787–3797.

https://doi.org/10.1016/j.ijsolstr.2014.07.014

40. Kim J-H, Paulino GH (2004) Simulation of Crack Propagation in Functionally Graded Materials Under Mixed-Mode and Non-Proportional Loading. Int J Mech Mater Des 1:63–94. https://doi.org/10.1023/b:mamd.0000035457.78797.c5

41. Kirugulige M, Tippur H V. (2008) Mixed-mode dynamic crack growth in a functionally graded particulate composite: Experimental measurements and finite element simulations. In: Journal of Applied Mechanics, Transactions ASME. pp 0511021–05110214

42. Silling SA (2000) Reformulation of elasticity theory for discontinuities and long-range forces. J Mech Phys Solids 48:175–209. https://doi.org/10.1016/S0022-5096(99)00029-0

43. Silling SA, Askari E (2005) A meshfree method based on the peridynamic model of solid mechanics. Comput Struct 83:1526–1535. https://doi.org/10.1016/j.compstruc.2004.11.026

44. Silling SA, Lehoucq RB (2008) Convergence of peridynamics to classical elasticity theory. J Elast 93:13–37. https://doi.org/10.1007/s10659-008-9163-3

45. Oterkus E, Madenci E, Weckner O, et al (2012) Combined finite element and peridynamic analyses for predicting failure in a stiffened composite curved panel with a central slot. Compos Struct 94:839–850. https://doi.org/10.1016/j.compstruct.2011.07.019

46. Liu S, Fang G, Liang J, Lv D (2020) A coupling model of XFEM/peridynamics for 2D dynamic crack propagation and branching problems. Theor Appl Fract Mech 108:. https://doi.org/10.1016/j.tafmec.2020.102573

47. De Meo D, Russo L, Oterkus E (2017) Modeling of the onset, propagation, and interaction of multiple cracks generated from corrosion pits by using peridynamics. J Eng Mater Technol Trans ASME 139:1–9. https://doi.org/10.1115/1.4036443

48. Bang DJ, Madenci E (2017) Peridynamic modeling of hyperelastic membrane deformation. J Eng Mater Technol Trans ASME 139:. https://doi.org/10.1115/1.4035875

49. De Meo D, Zhu N, Oterkus E (2016) Peridynamic modeling of granular fracture in polycrystalline materials. J Eng Mater Technol Trans ASME 138:. https://doi.org/10.1115/1.4033634

50. Diyaroglu C, Oterkus E, Madenci E, et al (2016) Peridynamic modeling of composite laminates under explosive loading. Compos Struct 144:14–23. https://doi.org/10.1016/j.compstruct.2016.02.018

51. Javili A, McBride AT, Steinmann P (2021) A geometrically exact formulation of peridynamics. Theor Appl Fract Mech 111:102850. https://doi.org/10.1016/j.tafmec.2020.102850

52. Nguyen CT, Oterkus S (2021) Ordinary state-based peridynamics for geometrically nonlinear analysis of plates. Theor Appl Fract Mech 112:. https://doi.org/10.1016/j.tafmec.2020.102877

53. Nguyen CT, Oterkus S, Oterkus E (2021) A physics-guided machine learning model for two-dimensional structures based on ordinary state-based peridynamics. Theor Appl Fract Mech 112:102872. https://doi.org/10.1016/j.tafmec.2020.102872

54. Dai MJ, Tanaka S, Oterkus S, Oterkus E (2020) Mixed-mode stress intensity factors evaluation of flat shells under in-plane loading employing ordinary state-based peridynamics. Theor Appl Fract Mech 102841. https://doi.org/10.1016/j.tafmec.2020.102841

55. Shou Y, Zhou X, Berto F (2019) 3D numerical simulation of initiation, propagation and coalescence of cracks using the extended non-ordinary state-based peridynamics. Theor Appl Fract Mech 101:254–268. https://doi.org/10.1016/j.tafmec.2019.03.006

56. Karpenko O, Oterkus S, Oterkus E (2021) Peridynamic Investigation of the Effect of Porosity on Fatigue Nucleation for Additively Manufactured Titanium Alloy Ti6Al4V. Theor Appl Fract Mech 102925. https://doi.org/10.1016/j.tafmec.2021.102925

57. Bang DJ, Ince A, Oterkus E, Oterkus S (2021) Crack growth modeling and simulation of a peridynamic fatigue model based on numerical and analytical solution approaches. Theor Appl Fract Mech 103026. https://doi.org/10.1016/j.tafmec.2021.103026

58. Yang Z, Oterkus E, Oterkus S (2021) Peridynamic modelling of higher order functionally graded plates. Math Mech Solids 1–23. https://doi.org/10.1177/10812865211004671

59. Madenci E, Oterkus E (2014) Peridynamic theory and its applications. Springer New York, New York, NY

60. Javili A, Morasata R, Oterkus E, Oterkus S (2019) Peridynamics review. Math Mech Solids 24:3714–3739. https://doi.org/10.1177/1081286518803411

61. Rubinstein AA (1985) Macrocrack interaction with semi-infinite microcrack array. Int J Fract 27:113–119. https://doi.org/10.1007/BF00040390

62. ROSE LRF (1986) Effective Fracture Toughness of Microcracked Materials. J Am Ceram Soc 69:212–214. https://doi.org/10.1111/j.1151-2916.1986.tb07409.x

63. Brencich A, Carpinteri A (1998) Stress field interaction and strain energy distribution between a stationary main crack and its process zone. Eng Fract Mech 59:797–814. https://doi.org/10.1016/S0013-7944(97)00158-6

64. Petrova V, Schmauder S (2011) Thermal fracture of a functionally graded/homogeneous bimaterial with system of cracks. Theor Appl Fract Mech 55:148–157. https://doi.org/10.1016/j.tafmec.2011.04.005

65. Singh I V., Mishra BK, Bhattacharya S (2011) XFEM simulation of cracks, holes and inclusions in functionally graded materials. Int J Mech Mater Des 7:199–218. https://doi.org/10.1007/s10999-011-9159-1

66. Vazic B, Wang H, Diyaroglu C, et al (2017) Dynamic propagation of a macrocrack interacting with parallel small cracks. AIMS Mater Sci 4:118–136. https://doi.org/10.3934/matersci.2017.1.118

67. Basoglu MF, Zerin Z, Kefal A, Oterkus E (2019) A computational model of peridynamic theory for deflecting behavior of crack propagation with micro-cracks. Comput Mater Sci 162:33–46. https://doi.org/10.1016/j.commatsci.2019.02.032

68. Cheng Z, Zhang G, Wang Y, Bobaru F (2015) A peridynamic model for dynamic fracture in functionally graded materials. Compos Struct 133:529–546. https://doi.org/10.1016/j.compstruct.2015.07.047

69. Cheng Z, Liu Y, Zhao J, et al (2018) Numerical simulation of crack propagation and branching in functionally graded materials using peridynamic modeling. Eng Fract Mech 191:13–32. https://doi.org/10.1016/j.engfracmech.2018.01.016

70. Cheng ZQ, Sui ZB, Yin H, et al (2019) Studies of dynamic fracture in functionally graded materials using peridynamic modeling with composite weighted bond. Theor Appl Fract Mech 103:102242. https://doi.org/10.1016/j.tafmec.2019.102242

71. Pathrikar A, Tiwari SB, Arayil P, Roy D (2021) Thermomechanics of damage in brittle solids: A peridynamics model. Theor Appl Fract Mech 112:. https://doi.org/10.1016/j.tafmec.2020.102880

72. Xia W, Oterkus E, Oterkus S (2021) Ordinary state-based peridynamic homogenization of periodic micro-structured materials. Theor Appl Fract Mech 113:102960.

https://doi.org/10.1016/j.tafmec.2021.102960

73. Ghajari M, Iannucci L, Curtis P (2014) A peridynamic material model for the analysis of dynamic crack propagation in orthotropic media. Comput Methods Appl Mech Eng 276:431–452. https://doi.org/10.1016/j.cma.2014.04.002

74. Ozdemir M, Kefal A, Imachi M, et al (2020) Dynamic fracture analysis of functionally graded materials using ordinary state-based peridynamics. Compos Struct 244:112296. https://doi.org/10.1016/j.compstruct.2020.112296

75. He D, Huang D, Jiang D (2021) Modeling and studies of fracture in functionally graded materials under thermal shock loading using peridynamics. Theor Appl Fract Mech 111:. https://doi.org/10.1016/j.tafmec.2020.102852

76. Candaş A, Oterkus E, İmrak CE (2021) Dynamic Crack Propagation and Its Interaction With Micro-Cracks in an Impact Problem. J Eng Mater Technol 143:1–10. https://doi.org/10.1115/1.4047746

77. Kalthoff JF, Winkler S (1987) Failure mode transition at high rates of loading. Impact Load Dyn Behav Mater 1:185–195

78. Kalthoff JF (2000) Modes of dynamic shear failure in solids. Int J Fract 101:1–31. https://doi.org/10.1023/a:1007647800529

79. Silling SA (2003) Dynamic fracture modeling with a meshfree peridynamic code. In: Computational Fluid and Solid Mechanics 2003. pp 641–644

80. Ren H, Zhuang X, Cai Y, Rabczuk T (2016) Dual-horizon peridynamics. Int J Numer Methods Eng 108:1451–1476. https://doi.org/10.1002/nme.5257

81. Ren H, Zhuang X, Rabczuk T (2017) Dual-horizon peridynamics: A stable solution to

varying horizons. Comput Methods Appl Mech Eng 318:762–782. https://doi.org/10.1016/j.cma.2016.12.031

82. Amani J, Oterkus E, Areias P, et al (2016) A non-ordinary state-based peridynamics formulation for thermoplastic fracture. Int J Impact Eng 87:83–94. https://doi.org/10.1016/j.ijimpeng.2015.06.019

83. Gu X, Zhang Q, Xia X (2017) Voronoi-based peridynamics and cracking analysis with adaptive refinement. Int J Numer Methods Eng 112:2087–2109. https://doi.org/10.1002/nme.5596

84. Guo JS, Gao WC (2019) Study of the Kalthoff–Winkler experiment using an ordinary state-based peridynamic model under low velocity impact. Adv Mech Eng 11:168781401985256. https://doi.org/10.1177/1687814019852561

85. Trask N, You H, Yu Y, Parks ML (2019) An asymptotically compatible meshfree quadrature rule for nonlocal problems with applications to peridynamics. Comput Methods Appl Mech Eng 343:151–165. https://doi.org/10.1016/j.cma.2018.08.016

86. Wang H, Xu Y, Huang D (2019) A non-ordinary state-based peridynamic formulation for thermo-visco-plastic deformation and impact fracture. Int J Mech Sci 159:336–344. https://doi.org/10.1016/j.ijmecsci.2019.06.008

87. Silling SA, Epton M, Weckner O, et al (2007) Peridynamic states and constitutive modeling. J Elast 88:151–184. https://doi.org/10.1007/s10659-007-9125-1

88. Zhang Z, Paulino GH, Celes W (2008) Cohesive modeling of dynamic crack growth in homogeneous and functionally graded materials. AIP Conf Proc 973:562–567. https://doi.org/10.1063/1.2896840

89. Stukowski A (2010) Visualization and analysis of atomistic simulation data with OVITO-the Open Visualization Tool. Model Simul Mater Sci Eng 18:. https://doi.org/10.1088/0965-0393/18/1/015012

90. Kalthoff JF (1988) Shadow Optical Analysis Of Dynamic Shear Fracture. Opt Eng 27:. https://doi.org/10.1117/12.7976772

91. Kalthoff JF (2003) Failure methodology of mode-II loaded cracks. Strength, Fract Complex 1:121–138

92. Loehnert S, Belytschko T (2007) Crack shielding and amplification due to multiple microcracks interacting with a macrocrack. Int J Fract 145:1–8. https://doi.org/10.1007/s10704-007-9094-1

93. Bleyer J, Roux-Langlois C, Molinari JF (2017) Dynamic crack propagation with a variational phase-field model: limiting speed, crack branching and velocity-toughening mechanisms. Int J Fract 204:79–100. https://doi.org/10.1007/s10704-016-0163-1

Table captions

Table 1 The homogeneous and FGM models' material properties

Figure captions

Fig. 1 The reference and deformed states for two material points

Fig. 2 Two different material points and broken bonds

Fig. 3 Determining average values for each bond in FGMs

Fig. 4 Geometrical details of Kalthoff-Winkler problem

Fig. 5 Crack paths and damages in models (a) M1 at 87.0 μs, (b) M1 at 104.4 μs, (c) M2 at 87.0 μs, (d) M2 at 104.4 μs, (e) M3 at 87.0 μs, (f) M3 at 104.4 μs. CL and y are crack length and *y*-coordinates of crack ends

Fig. 6 Crack velocity profiles of models M1, M2, M3, M4, and M5 between 26.1 and 91.4 μs

Fig. 7 Crack paths and damages in models (a) M1 at 91.4 μs, (b) M1 at 95.7 μs, (c) M4 at 91.4 μs, (d) M4 at 95.7 μs, (e) M5 at 91.4 μs, (f) M5 at 95.7 μs. CL and y are crack length and *y*-coordinates of crack ends

Fig. 8 Variation of material properties of M6 and M7 models across the height of the body, (a) Linear curve fits for Young's Modulus and density (b) Fracture energy, (same as those used in M8 and M9 models, respectively.)

Fig. 9 Crack paths and damages in models (a) M1 at 91.4 μs, (b) M1 at 100.1 μs, (c) M6 at 91.4 μs, (d) M6 at 100.1 μs, (e) M7 at 91.4 μs, (f) M7 at 100.1 μs. CL and y are crack length and *y*-coordinates of crack ends

Fig. 10 Crack velocity profiles of models M1, M6, and M7 between 26.1 and 91.4 μs

Fig. 11 Crack paths and damages in models (a) M1 at 91.4 μs, (b) M1 at 100.1 μs, (c) M8 at 91.4 μs, (d) M8 at 100.1 μs, (e) M9at 91.4 μs, (f) M9 at 100.1 μs. CL and y are crack length and *y*-coordinates of crack ends

Fig. 12 Crack velocity profiles of models M1, M6, M7, M8, M9, and M1-w/mc between 26.1 and 91.4 μs

Figures

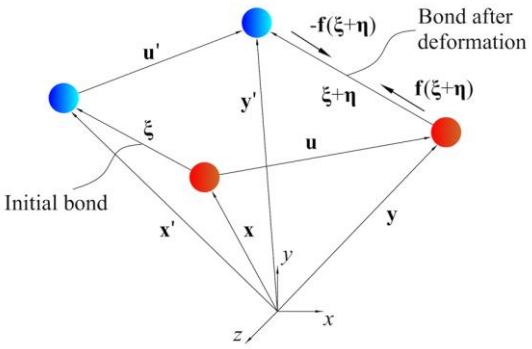

Fig.1 The reference and deformed states for two material points

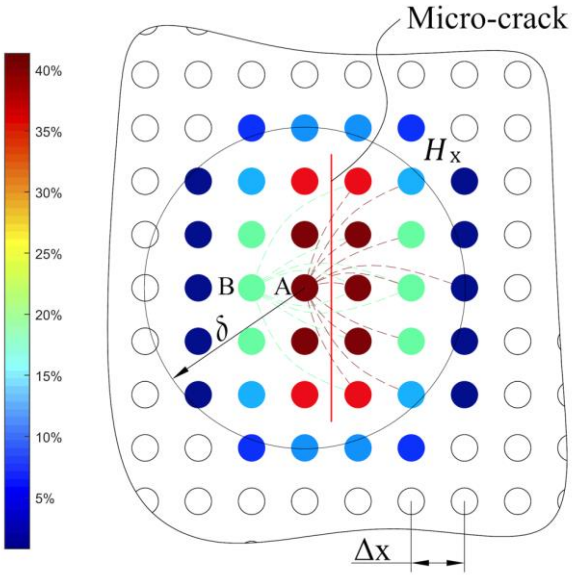

Fig.2 Two different material points and broken bonds

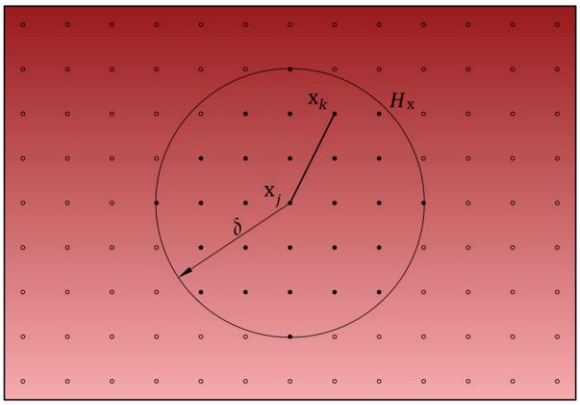

Fig. 3 Determining average values for each bond in FGMs

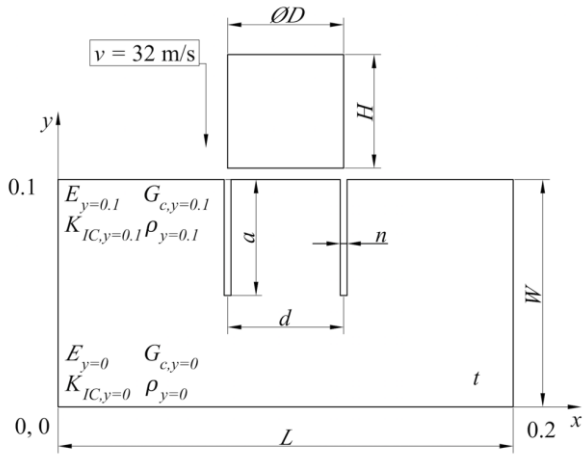

Fig. 4 Geometrical details of Kalthoff-Winkler problem

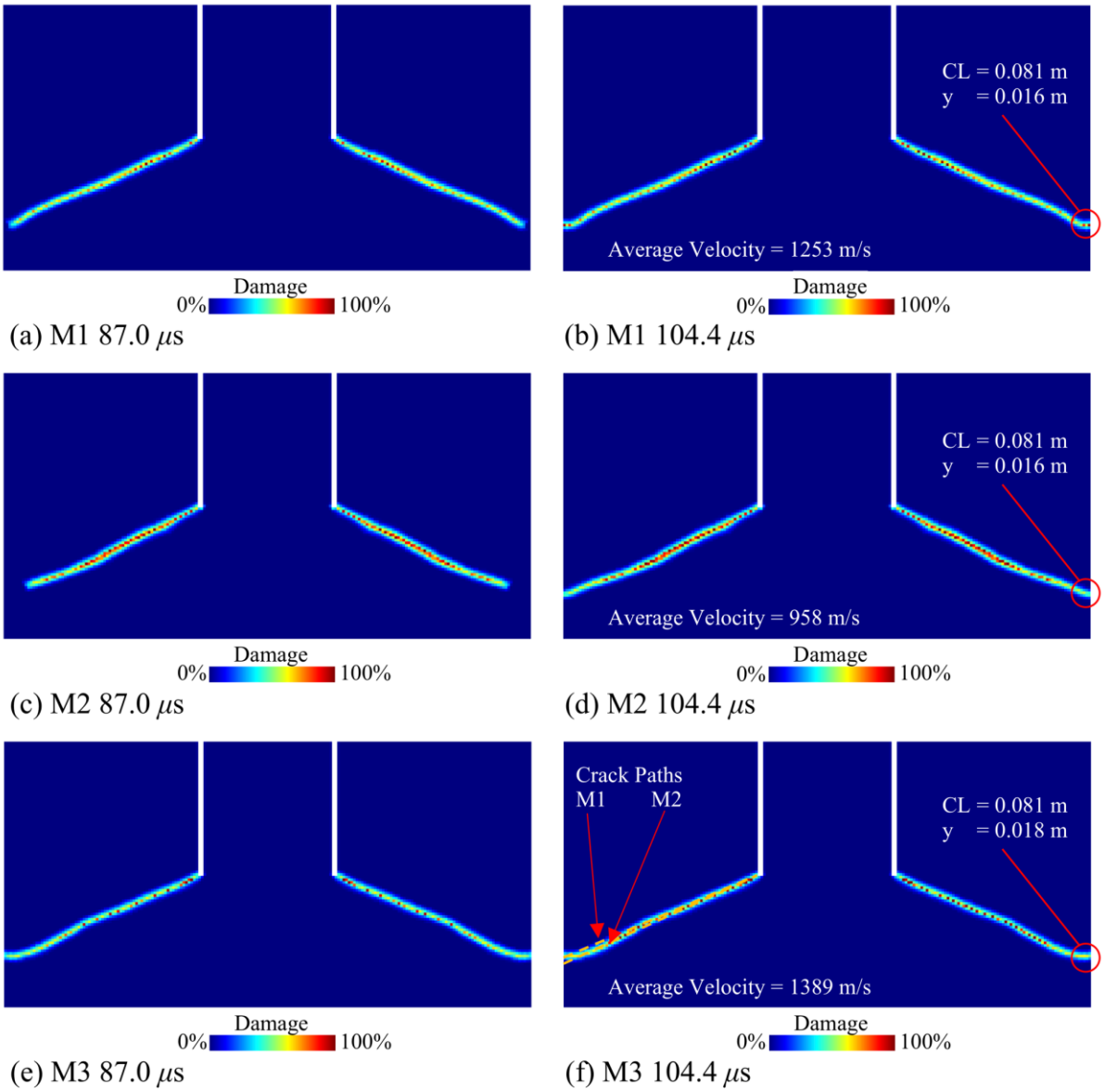

Fig. 5 Crack paths and damages in models (a) M1 at 87.0 μs, (b) M1 at 104.4 μs, (c) M2 at 87.0 μs, (d) M2 at 104.4 μs, (e) M3 at 87.0 μs, (f) M3 at 104.4 μs. CL and y are crack length and y-coordinates of crack ends

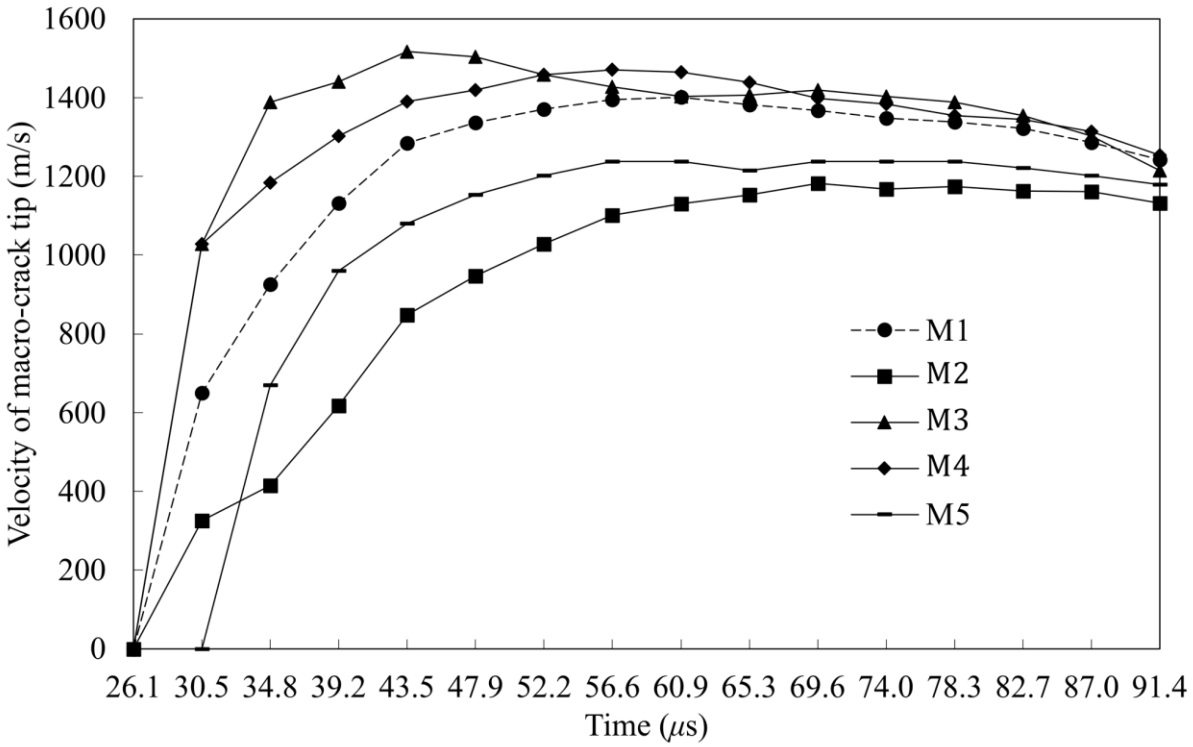

Fig. 6 Crack velocity profiles of models M1, M2, M3, M4, and M5 between 26.1 and 91.4 μs

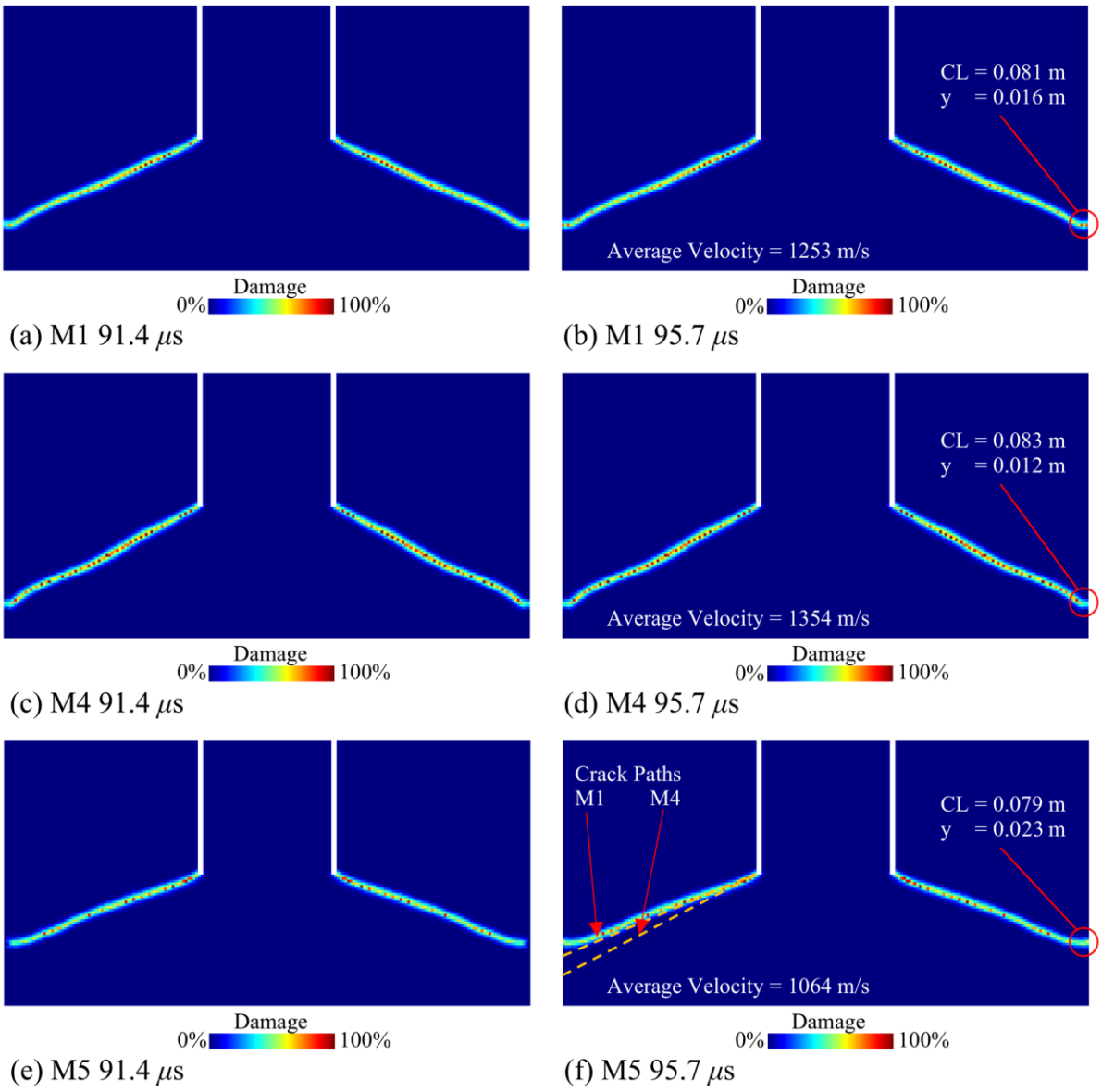

Fig. 7 Crack paths and damages in models (a) M1 at 91.4 μs, (b) M1 at 95.7 μs, (c) M4 at 91.4 μs, (d) M4 at 95.7 μs, (e) M5 at 91.4 μs, (f) M5 at 95.7 μs. CL and y are crack length and y-coordinates of crack ends

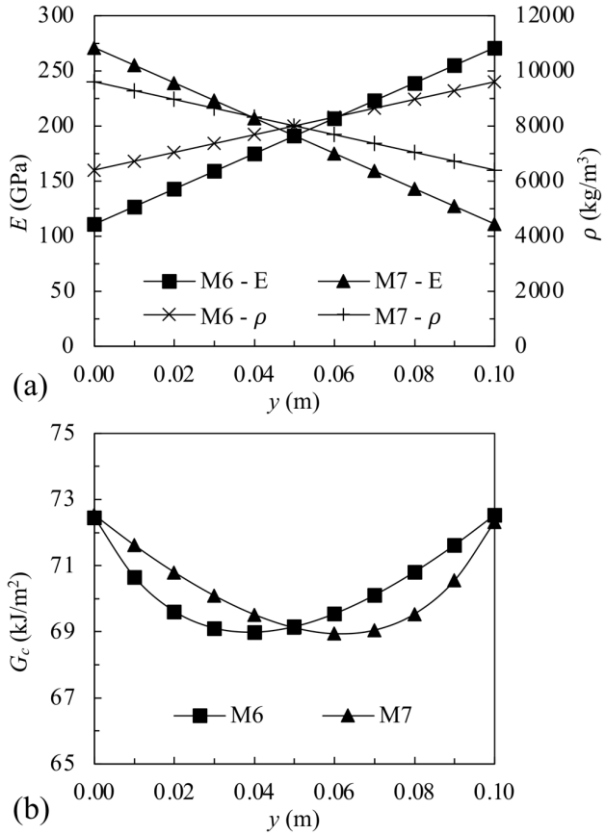

Fig. 8 Variation of material properties of M6 and M7 models across the height of the body, (a) Linear curve fits for Young's Modulus and density (b) Fracture energy, (M8 and M9 models have same material properties as M6 and M7, respectively.)

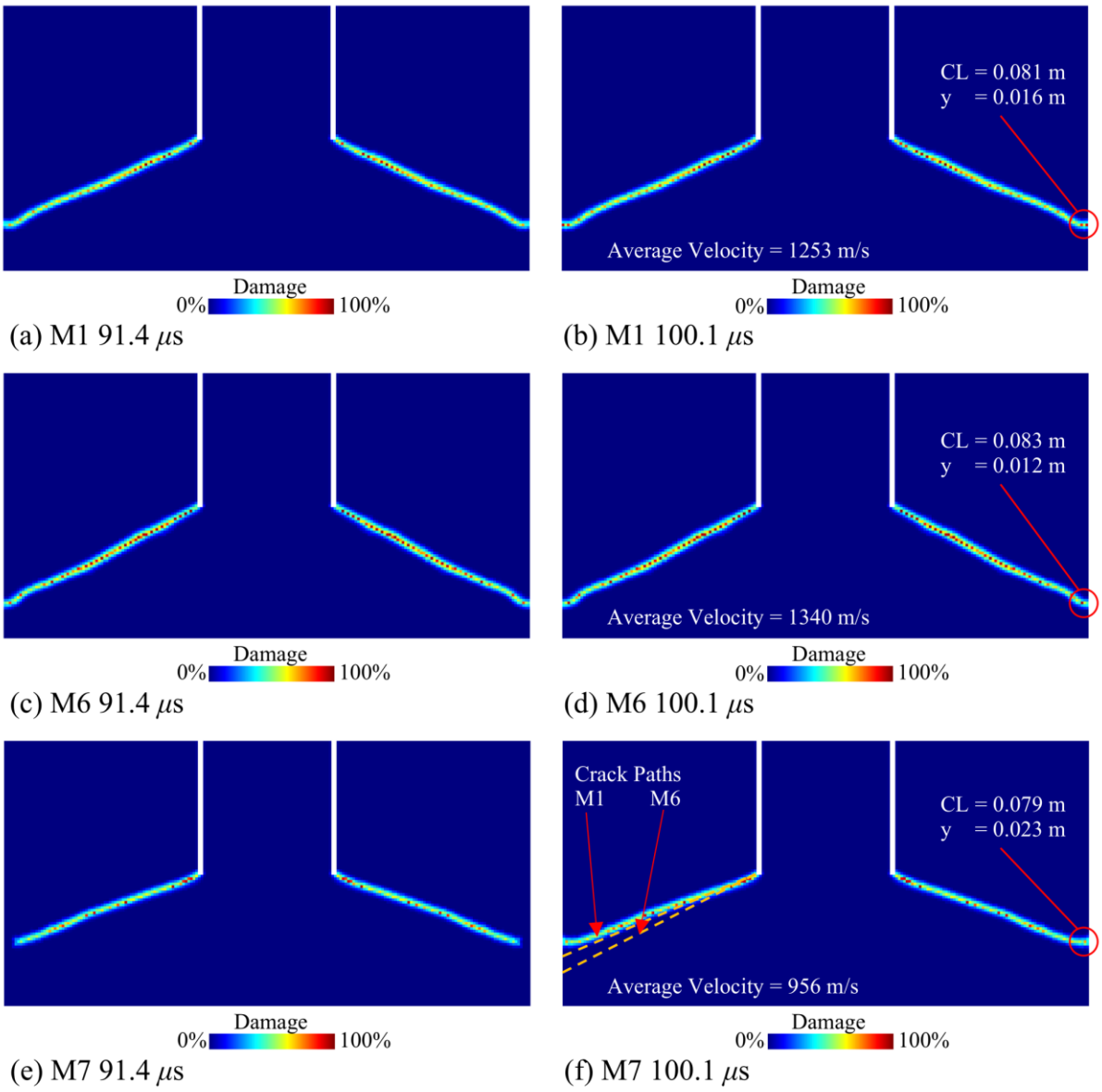

Fig. 9 Crack paths and damages in models (a) M1 at 91.4 μs, (b) M1 at 100.1 μs, (c) M6 at 91.4 μs, (d) M6 at 100.1 μs, (e) M7 at 91.4 μs, (f) M7 at 100.1 μs. CL and y are crack length and y-coordinates of crack ends

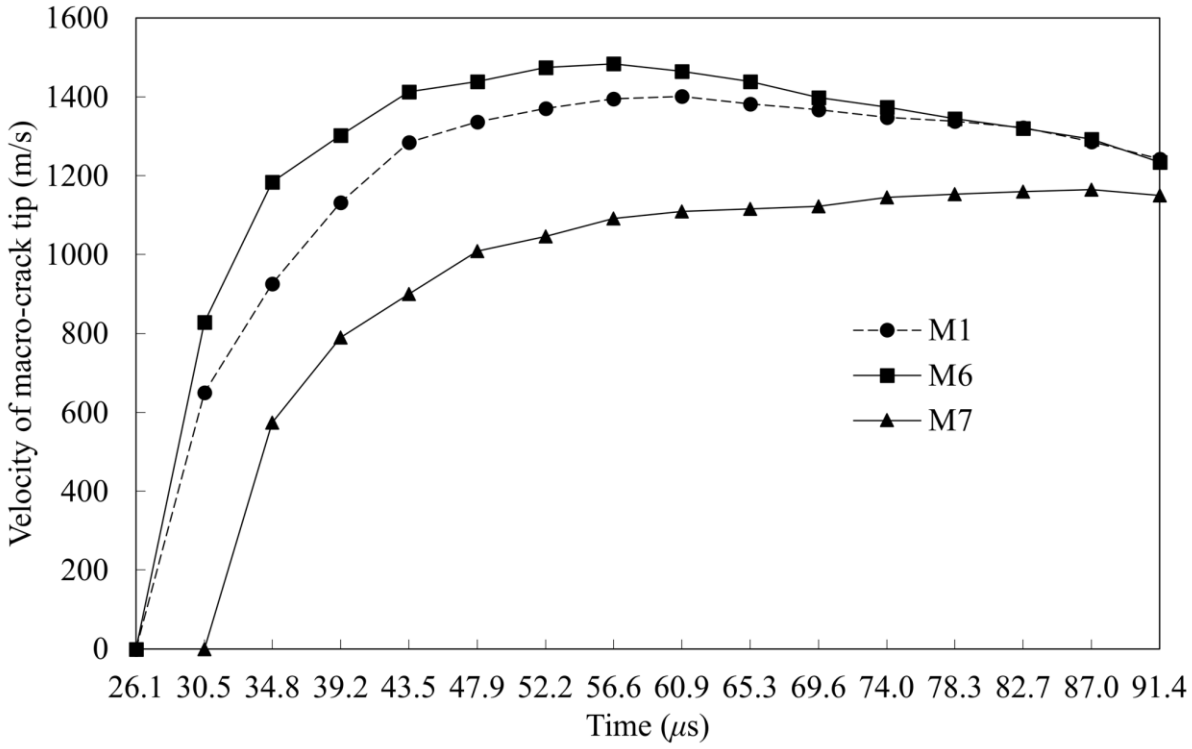

Fig. 10. Crack velocity profiles of models M1, M6, and M7 between 26.1 and 91.4 μs

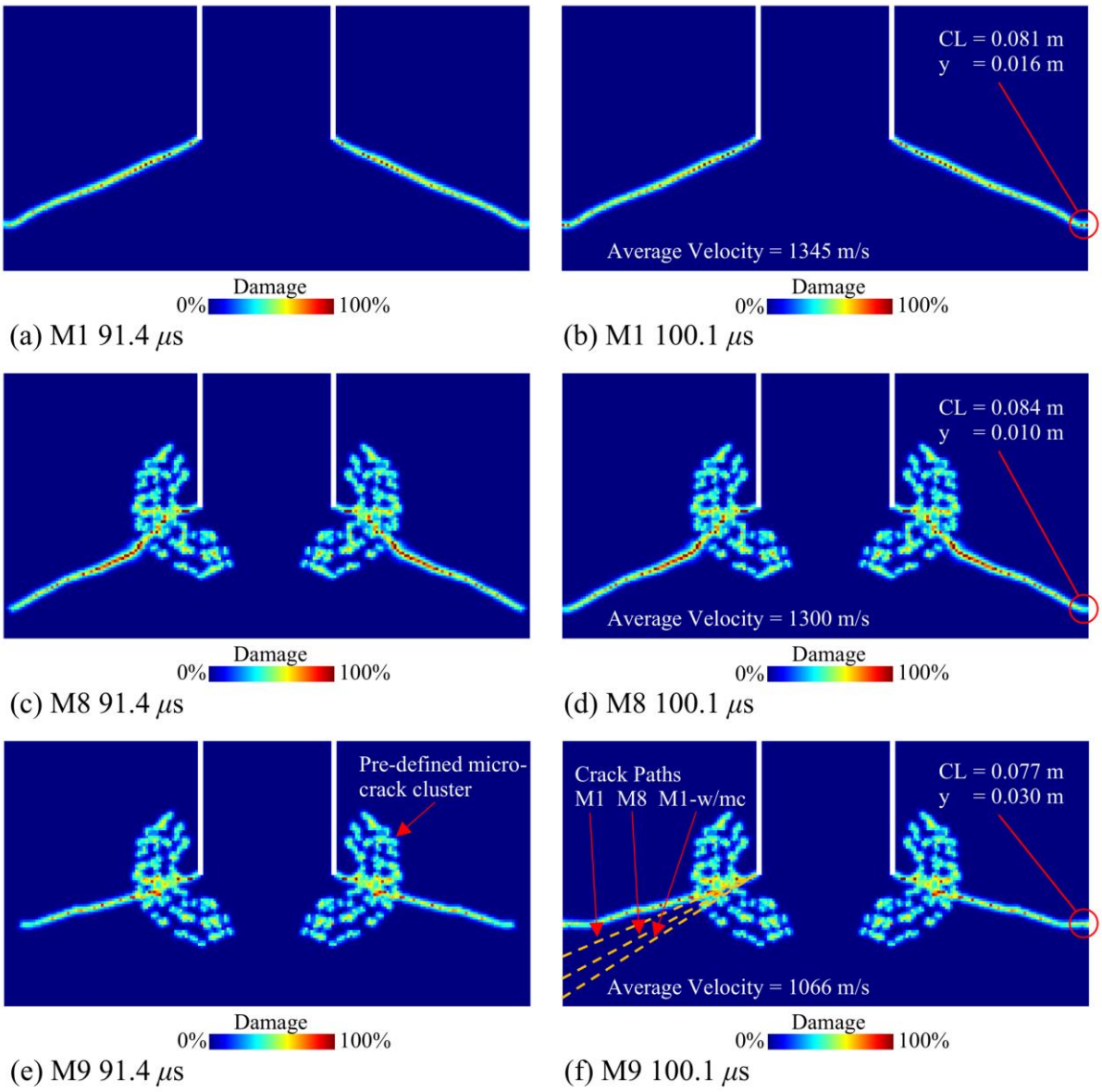

Fig. 11 Crack paths and damages in models (a) M1 at 91.4 μs, (b) M1 at 100.1 μs, (c) M8 at 91.4 μs, (d) M8 at 100.1 μs, (e) M9at 91.4 μs, (f) M9 at 100.1 μs. CL and y are crack length and y-coordinates of crack ends

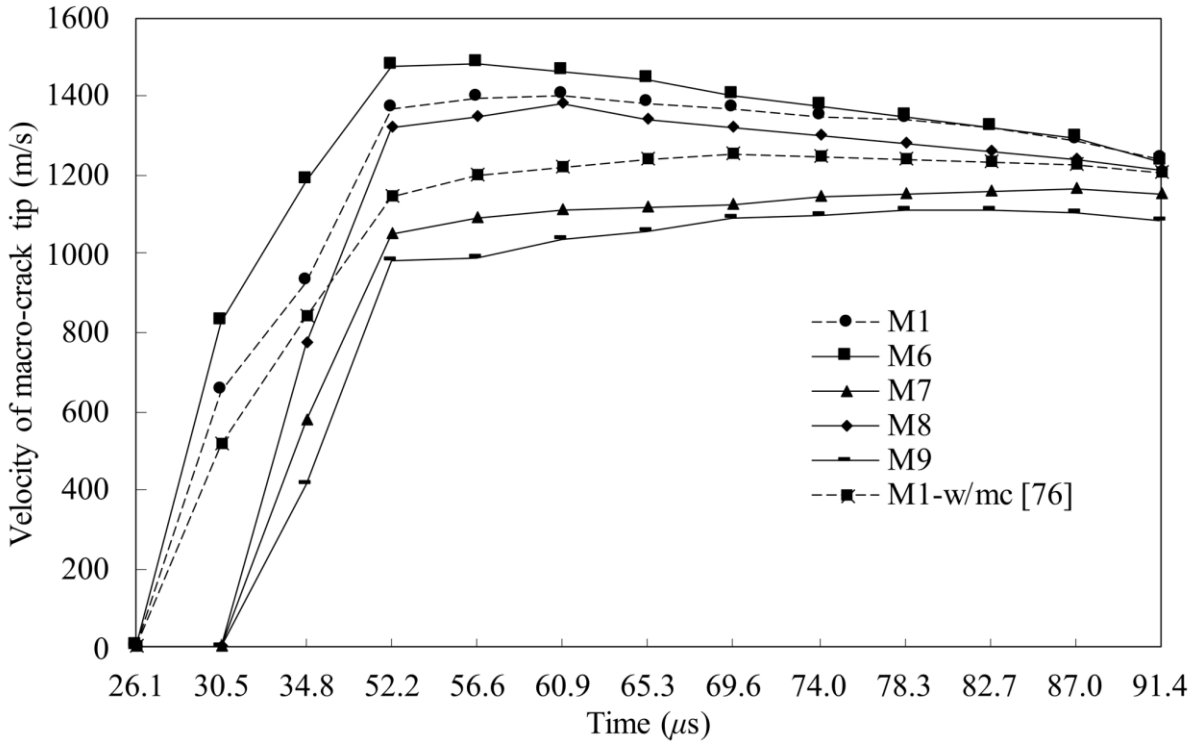

Fig. 12 Crack velocity profiles of models M1, M6, M7, M8, M9, and M1-w/mc between 26.1 and 91.4 μs

Table 1 The homogeneous and FGM models' material properties

	Young's Modulus (GPa)		Critical Energy Release Rate (kJ/m^2)		Fracture Toughness (MPa m$^{1/2}$)		Mass Density (kg/m^3)	
	$E_{y=0}$	$E_{y=0.1}$	$G_{c,y=0}$	$G_{c,y=0.1}$	$K_{IC,y=0}$	$K_{IC,y=0.1}$	$\rho_{y=0}$	$\rho_{y=0.1}$
M1 (Ref. Model)	191	191	69.1	69.1	114.9	114.9	8000	8000
M2	127	127	46.1	46.1	76.5	76.5	8000	8000
M3	255	255	92.1	92.1	153.2	153.2	8000	8000
M4	127	255	46.1	92.1	76.5	153.2	8000	8000
M5	255	127	92.1	46.1	153.2	76.5	8000	8000
M6	111	271	52.7	86.6	76.5	153.2	6400	9600
M7	271	111	86.6	52.7	153.2	76.5	9600	6400
M8	111	271	52.7	86.6	76.5	153.2	6400	9600
M9	271	111	86.6	52.7	153.2	76.5	9600	6400